

Ad-hoc vibration monitoring system for a stress-ribbon footbridge: from design to operation

Norberto Iban^{1a}, Jose M. Soria^{2b}, Alvaro Magdaleno^{*3}, Carlos Casado^{1c},
Ivan M. Diaz^{2d} and Antolin Lorenzana^{3e}

¹Centro Tecnológico CARTIF, Parque Tecnológico de Boecillo, 47151 Valladolid, Spain

²E.T.S. de Ingenieros de Caminos, Canales y Puertos, Universidad Politécnica de Madrid,
Calle del Profesor Aranguren 3, 28040 Madrid, Spain

³ITAP, Escuela de Ingenierías Industriales, Universidad de Valladolid, Paseo del Cauce 59, 47011 Valladolid, Spain

(Received January 31, 2017, Revised March 29, 2018, Accepted April 19, 2018)

Abstract. Pedro Gómez Bosque footbridge is a slender and lightweight structure that creates a pedestrian link over the Pisuerga River, Valladolid, Spain. This footbridge is a singular stress ribbon structure with one span of 85 m consisting on a steel plate and precast concrete slabs laying on it. Rubber pavement and a railing made of stainless steel and glass complete the footbridge. Because of its lively dynamics, prone to oscillate, a simple and affordable structural health monitoring system was installed in order to continuously evaluate its structural serviceability and to estimate its modal parameters. Once certain problems (conditioning and 3D orientation of the triaxial accelerometers) are overcome, the monitoring system is validated by comparison with a general purpose laboratory portable analyzer. Representative data is presented, including acceleration magnitudes and modal estimates. The evolution of these parameters has been analysed over one-year time.

Keywords: SHM; serviceability assessment; structural dynamics; modal parameters

1. Introduction

This work describes the design, installation and initial operation of a remotely controlled continuous vibration monitoring system on a footbridge. The singularity of the structure, its slenderness and the prescription of not affecting to its aesthetic in any way, together with cost restrictions, lead to the decision of designing low-cost MEMS-based triaxial accelerometers properly conditioned and embedded inside the handrail as structural vibration sensors. The monitoring system was validated by comparing the data measured by the MEMS accelerometers with conventional piezoelectric accelerometers. These tests demonstrated that these sensors are a competitive alternative to traditional ones and that the system is ready to be used for the dynamic characterization of the structure and to integrate a continuous structural health assessment

and serviceability analysis.

The use of traditional techniques for life cycle management together with structural health monitoring new techniques enables more accurate identification for optimal maintenance strategies for a wide range of limit states (Orcesi *et al.* 2010). The long-term monitoring provides the best method to understand and quantify the real environmental loading and the corresponding structure response.

Multiple examples of structures equipped with monitoring systems can be found (Brownjohn *et al.* 2010, Swartz *et al.* 2010, Gomez *et al.* 2011, Moser and Moaveni 2013, Casciati *et al.* 2014): chimneys, wind turbines, masonry towers, bridges, footbridges, etc. The main problem for wide-spreading the implementation of these monitoring systems is the cost associated to purchasing, installation of the measuring system (sensors, acquisition equipment, wires, ...) and its operation maintenance. Many authors have conducted studies that involve the use of wireless technologies in order to reduce costs associated to wiring and installation (Shinozuka *et al.* 2004, Chen and Casciati 2014, Tokognon *et al.* 2017). However, these systems usually suffer communication problems in large structures and under environmental hazards. Additionally, it is not always possible to ensure wireless communication between sensors and problems with battery life arisen when long-term monitoring is required. These problems have been tackled by using energy harvesting systems (Guan and Liao 2006, Chen 2014), but they have not reached sufficient maturity yet. Another option to reduce the cost of monitoring systems is the one chosen in the structure under study: to use low-cost wired sensors and data loggers. Other

*Corresponding author, Ph.D. Student

E-mail: alvaro.magdaleno@uva.es

^a Ph.D. Student

E-mail: noriba@catif.es

^b Ph.D. Student

E-mail: jm.soria@upm.es

^c Ph.D. Student

E-mail: carcas@cartif.es

^d Dr.

E-mail: ivan.munoz@upm.es

^e Dr.

E-mail: ali@eii.uva.es

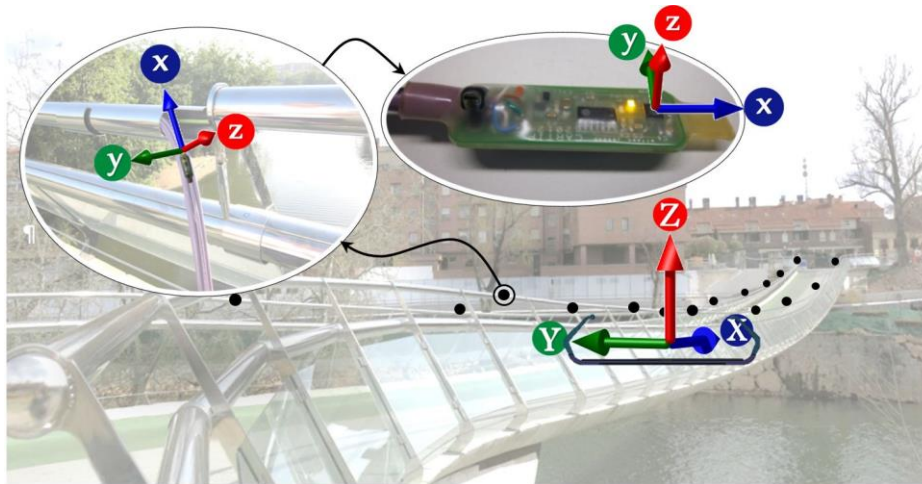


Fig. 1 Cross-section with the global axis, local axis for the MEMS accelerometers and their location (black points) in the footbridge

authors have also experienced with this kind of new promising technologies (Ceylan *et al.* 2013, Tan *et al.* 2011, Panigrahi *et al.* 2010, Caetano *et al.* 2011) in increasing development during the last decade.

2. Structure description

Pedro Gómez Bosque footbridge (see Fig. 1) mainly consists of a corten steel sheet of 94 m long, 3.6 m width and only 30 mm thick which is pre-tensioned and anchored to the two abutments, which are 85 m apart and 2 m not on a level. The complete steel sheet was on-site manufactured welding together 8-meter long plates. Precast concrete slabs of 5.2 m long, 0.75 m width and around 120 mm thick lay on the steel sheet. These slabs do not have bearing mission, that is, the only structural element between abutments is the steel sheet. The structure is completed by rubber pavement and a stainless steel and glass railing. More information about the structure can be seen in Narros (2011). All these structural and non-structural elements suppose, according to the project, a dead load around $\omega = 23.6$ kN/m. Initial pre-tension on the steel sheet was adjusted so that, at the reference temperature (20°C), displacement in the middle (sag) were limited to $L/50$ which means 1.7 m. Using indirect computations, an axial tension of $H = 12.54$ MN (in reference conditions) has been estimated so stresses in the steel are around 120 MPa. Considering a service overload of $\Delta\omega = 15.7$ KN/m and cold weather conditions, stresses could reach up to 192 MPa. Analytically estimated values for deflection (δ) and axial force (H) are presented in Table 1 for the relevant design conditions. Note that a change in 15°C supposes a thermal elongation of 17 mm leading to a change around 1.25 MN in the axial tension. Besides, as it is known (Strasky 2005, Lepidi and Gattulli 2012), the temperature not only affect to the static response but also to the frequency of the vibration modes, as Table 2 will show.

Table 1 Estimated static response for relevant project loading conditions

ω (kN/m)	Δt (°C)	δ (m)	H (MN)
23.6	0.0	1.70	12.54
23.6	-15.0	1.55	13.79
39.3	15.0	2.03	17.45
39.3	-15.0	1.77	20.03

A previous operational modal analysis was carried out using a portable lab system (consisting on 8 piezoelectric accelerometers MMF-KS48C, with 1000 mV/g sensitivity and low frequency ranges connected to a MGCplus HBM data logger through IEPE modules). Natural frequencies and mode shapes were estimated using standard SSI methodology. About twenty vibration modes, including vertical, lateral, torsional and coupled modes, were well identified between 0.8 and 10 Hz. This preliminary data is important to design the monitoring system and to choose the most appropriate technical specifications for the sensors and their number and location in the structure.

3. Monitoring system

From the functional and aesthetic point of view, the only possibility for installing the vibration sensors was to embed them into the 60 mm diameter CHS tube used as handrail. 18 triaxial accelerometers, 9 at each side of the deck, were positioned equidistant 10.625 m along the span (plotted with black points in Fig. 1). A temperature sensor, an anemometer and a vane installed in a nearby streetlight complete the system.

3.1 Sensors description, conditioning and installation

The vibration sensor chosen was the ADXL327 MEMS accelerometer developed by Analog Devices. The

ADXL327 is a very small, low power, 3-axis accelerometer with signal conditioned voltage outputs. It can measure the static acceleration of gravity in tilt-sensing applications as well as dynamic acceleration at high sampling frequencies. The accelerometer properties are initially suitable (measurement range up to ± 2.5 g, sensitivity up to 500 mV/g, bandwidth up to 550 Hz) to measure the expected dynamic response (in frequencies and in amplitudes) but it is not initially designed for long wire distances. To overcome this problem, MEMS device has been integrated in a circuit (Fig. 2) with other consumer electronic durables. First, a capacitor was placed in each axis in order to fix the measurement bandwidth to 100 Hz. Then, as the accelerometer has to be supplied by 3.6 V to get its nominal sensitivity of 500 mV/g, the power supply used is in 12 V and a voltage regulator to 3.6 V were integrated in the circuit board in order to avoid power losses by the long wires. As the impedance at each axis of the accelerometer output is high enough (32 k Ω) to cause noise problems by the long wires, an operational amplifier was added to reduce the impedance to 10 Ω and decrease the noise to 25 $\mu\text{g}/\sqrt{\text{Hz}}$. Also, a LED was included for power test. All the components, together with the end of its wire, are sealed using a thermo shrink-wrap plastic system (Fig. 1, right detail). The circuit resulting prototype is small enough (50 \times 17 \times 8 mm) for installing requirements.

Wires and sensors were immersed inside the handrail using a long wire guide. This fact introduced additional complications on the installation process as the orientation of the 3 axes of the sensor cannot be fixed beforehand. To overcome this problem, one of the axis of the triaxial accelerometer (x) was placed along the longitudinal direction of the board and its long side was aligned with the set of wires along the handrail (see left detail in Fig. 1), it can be assumed that the x-axis for all the sensor remains in the vertical plane (XZ), although no initial guess can be made about the spatial orientation of the other two axes (y and z). With this installing procedure, yaw angle around local z axis is prevented but a certain pitch (α) and roll (β) angles are still unknown (Fig. 3). A so called “static acceleration vector” $[\bar{a}_x, \bar{a}_y, \bar{a}_z]^t$ can be obtained averaging each axis register over enough time. Once transformed using the pitch and roll angles, this vector has to be the gravity vector $[0, 0, g]^t$, as shown in Eq. (1).

$$\begin{bmatrix} 0 \\ 0 \\ g \end{bmatrix} = \begin{bmatrix} \cos \alpha & 0 & \sin \alpha \\ 0 & 1 & 0 \\ -\sin \alpha & 0 & \cos \alpha \end{bmatrix} \cdot \begin{bmatrix} 1 & 0 & 0 \\ 0 & \cos \beta & \sin \beta \\ 0 & -\sin \beta & \cos \beta \end{bmatrix} \cdot \begin{bmatrix} \bar{a}_x \\ \bar{a}_y \\ \bar{a}_z \end{bmatrix} = [R] \cdot \begin{bmatrix} \bar{a}_x \\ \bar{a}_y \\ \bar{a}_z \end{bmatrix} \quad (1)$$

Solving the corresponding system of equations, it is possible to get α and β so matrix $[R]$ is known and acceleration vector in the global coordinate system $[a_x, a_y, a_z]^t$ (see Fig. 1), once removed the static value, can be obtained for any record $[a_x, a_y, a_z]^t$ using Eq. (2).

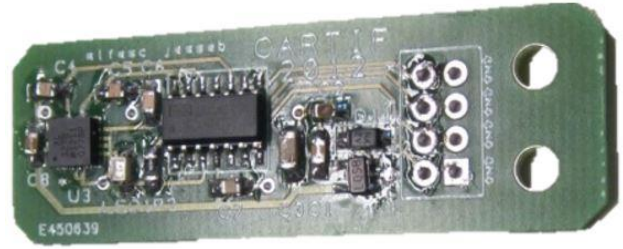


Fig. 2 Printed circuit board with all components

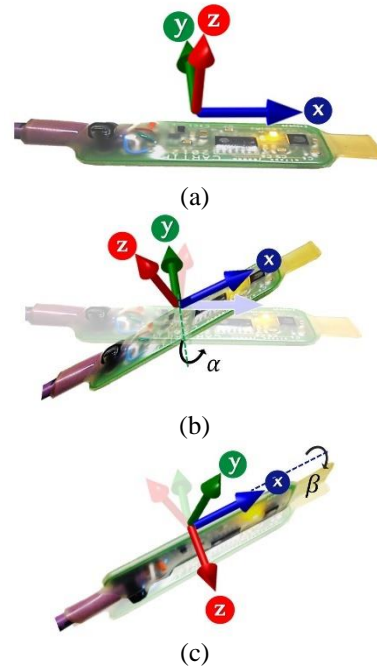


Fig. 3 Local x, y, z axis (a) in each board after a pitch, (b) and a roll and (c) rotations

$$\begin{bmatrix} a_x \\ a_y \\ a_z \end{bmatrix} = [R] \cdot \begin{bmatrix} \bar{a}_x \\ \bar{a}_y \\ \bar{a}_z \end{bmatrix} - \begin{bmatrix} 0 \\ 0 \\ g \end{bmatrix} \quad (2)$$

As an example, applying this procedure to the data shown in Fig. 4(a), where $[\bar{a}_x, \bar{a}_y, \bar{a}_z]^t = [1.30, 9.55, 1.83]^t$, the resulting angles are $\alpha = 7.61^\circ$ and $\beta = 100.85^\circ$. The transformed acceleration vector $[a_x, a_y, a_z]^t$ is shown in Fig. 4(b). The angular values obtained might change slightly with the temperature (note that the set of wires is free to move inside the handrail) and because of that they are recalculated hourly.

The temperature sensors used for the monitoring system was model T0110 transmitter Comet with range -30 to $+80^\circ\text{C}$ and accuracy $\pm 0.4^\circ\text{C}$. The wind sentry used was model 03002L from R. M. Young Company with range 0 to 50 m/s and accuracy ± 0.5 m/s for the speed and range 360° and accuracy ± 5 m/s for the direction.

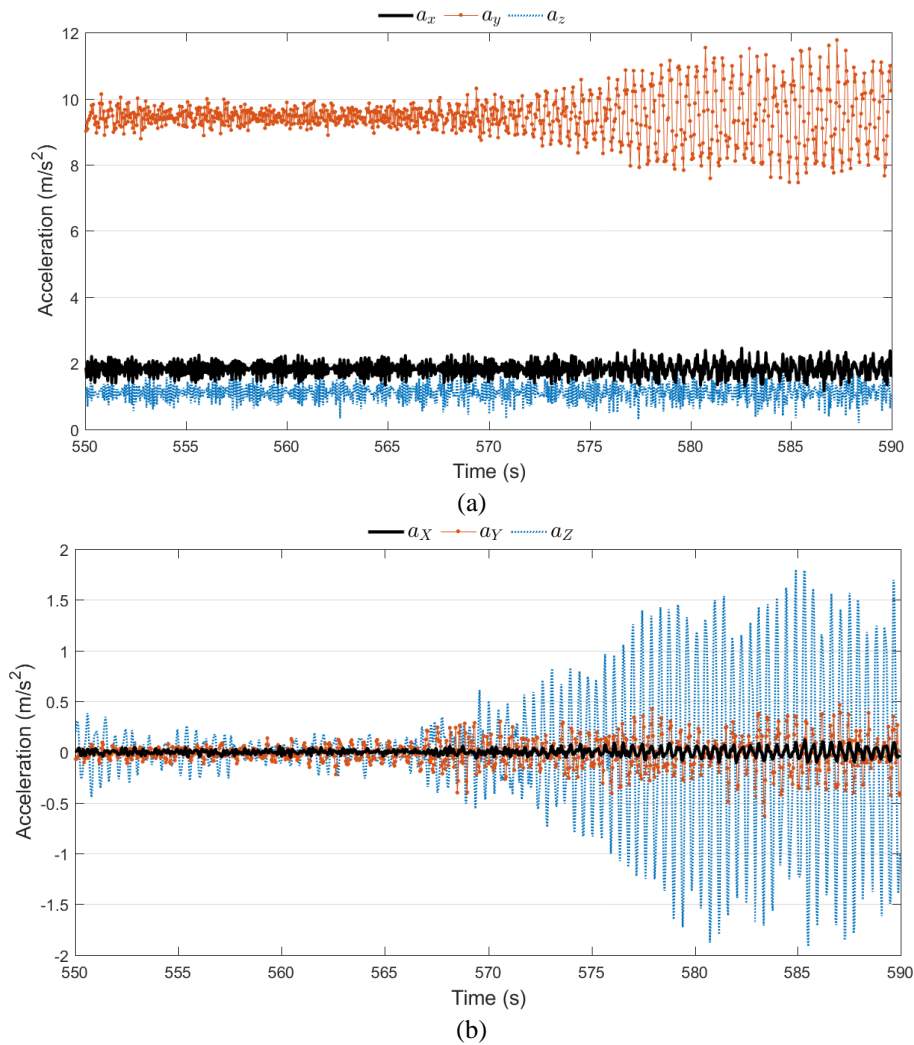


Fig. 4 Local x, y, z accelerations (a) and transformed ones (b) into the global axis (X, Y, Z)

3.2 Lab calibration

In order to calibrate the new devices and to evaluate their signal-to-noise ratio the following procedure was carried out. The portable lab system (equipped with the piezoelectric accelerometers) was placed together with the MEMS one connected to the longest wire (around 100~m). Both were located in a bending pinned beam (first mode at 2.27 Hz, free damped response after an impulsive load, 0.18% damping). Results are shown in Fig. 5. Note that, regardless technical specifications and the electronic conditioning, for amplitudes below 0.02 m/s² the noise is very evident and induce increments in the RMS values in more than 10%, so the use of the signal is limited. The three axis of each MEMS have the same amplitude calibration and signal-to-noise ratio. Same data-logger is used to record piezoelectric and MEMS signals. Even though, MEMS signal is 0.032 s delayed due to the MEMS electronic conditioning devices. This delay is the same for all the MEMS regardless the length of the wire, so this is not a problem for modal identification purposes if only MEMS accelerometers are used.

3.3 Data logger

As said before, the monitoring system comprises 18 triaxial accelerometers, a temperature sensor and an anemometer and vane in such a way that 57 voltage channels for the measurement system were needed. The data logger chosen was a CompactRIO 9076 from National Instruments with two 32 channels analogic input modules NI 9205. This data logger with a rugged hardware chassis has a stand-alone embedded control useful for real-time acquisition. The real-time processor is of 400 MHz and Ethernet, USB and RS232 connections are available in this model. The modules have 32 single-ended analogic inputs with 16-bit resolution, 250 kS/s aggregate sampling rate and voltage range from ± 200 mV to ± 10 V.

The frequency sampling for each channel is set to 200 Hz, enough to identify the modal parameters of the structure and to avoid aliasing problems (significant vibration modes have natural frequencies smaller than 10 Hz). A file with the recorded data is saved each hour in order to post-process them and to prevent measurement failures.

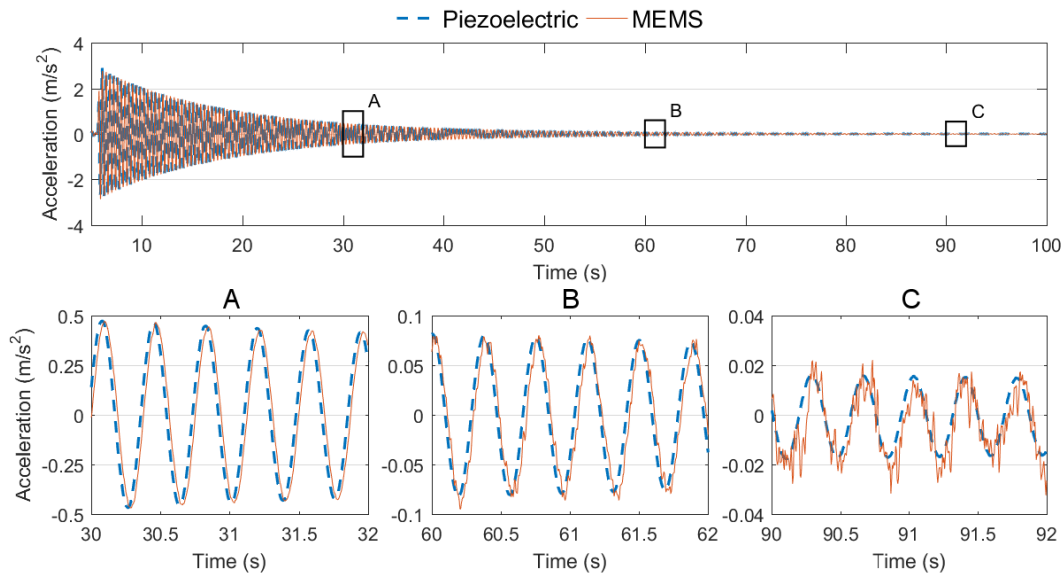


Fig. 5 Piezoelectric vs. MEMS devices

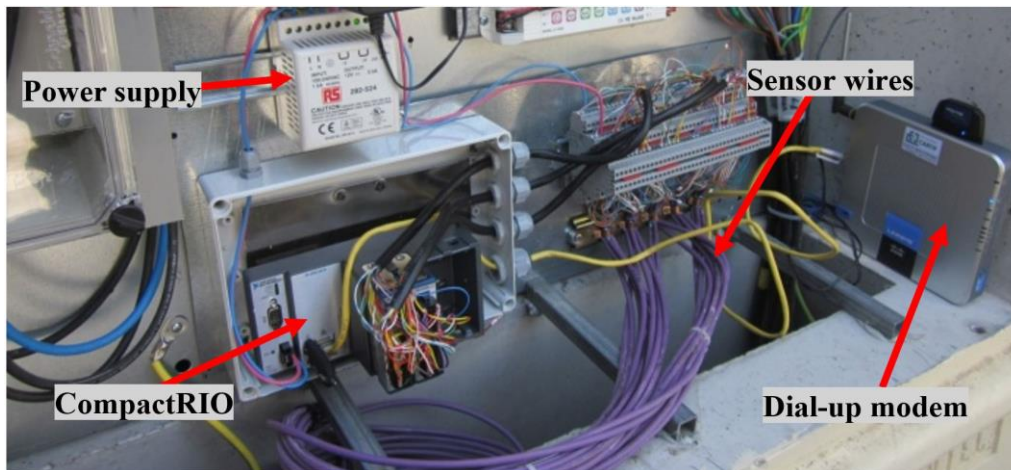


Fig. 6 Data logger, router and other devices

The two set of wires (one for each side of the railing) were long enough to reach the electrical cabinet sited near the footbridge where the data logger is installed. Fig. 6 shows the data logger and the two sets of wires, among other devices.

3.4 In-situ validation

Once the monitoring system was installed and ready to use, two additional checks were addressed. First, the location of each accelerometer was verified by lightly tapping on specific locations on the handrail, analyzing the response of the nearby accelerometers and identifying the one with more response, revealing its position accurately enough (around 120 mm). With this procedure was also possible to find out some failures with 3 accelerometer units from the downstream side.

After that, experimental tests were carried out to check the performance of these new system. The structural response was registered when groups of pedestrians walking over the deck, both with the portable system and also with the newly MEMS-based monitoring system (Fig. 7). The piezoelectric accelerometers were levelled to measure the structural vertical accelerations. These values were compared (Fig. 8) with the acceleration in Z axis registered with the A4 MEMS accelerometers (the nearest one, located around one third of the bridge span). The two recorded data sets are very similar in time and frequency domains. The only difference is that one new frequency appears (around 4.8 Hz) in the MEMS recordings. Those frequencies were identified as local natural frequencies for the handrail where MEMS are embedded. With the interest focused in modal identification and serviceability, the new frequencies are removed from the records after applying the corresponding band-stop filter.



Fig. 7 Test for the in-situ validation comparing piezoelectric (detail view) versus A4 MEMS (embedded) records

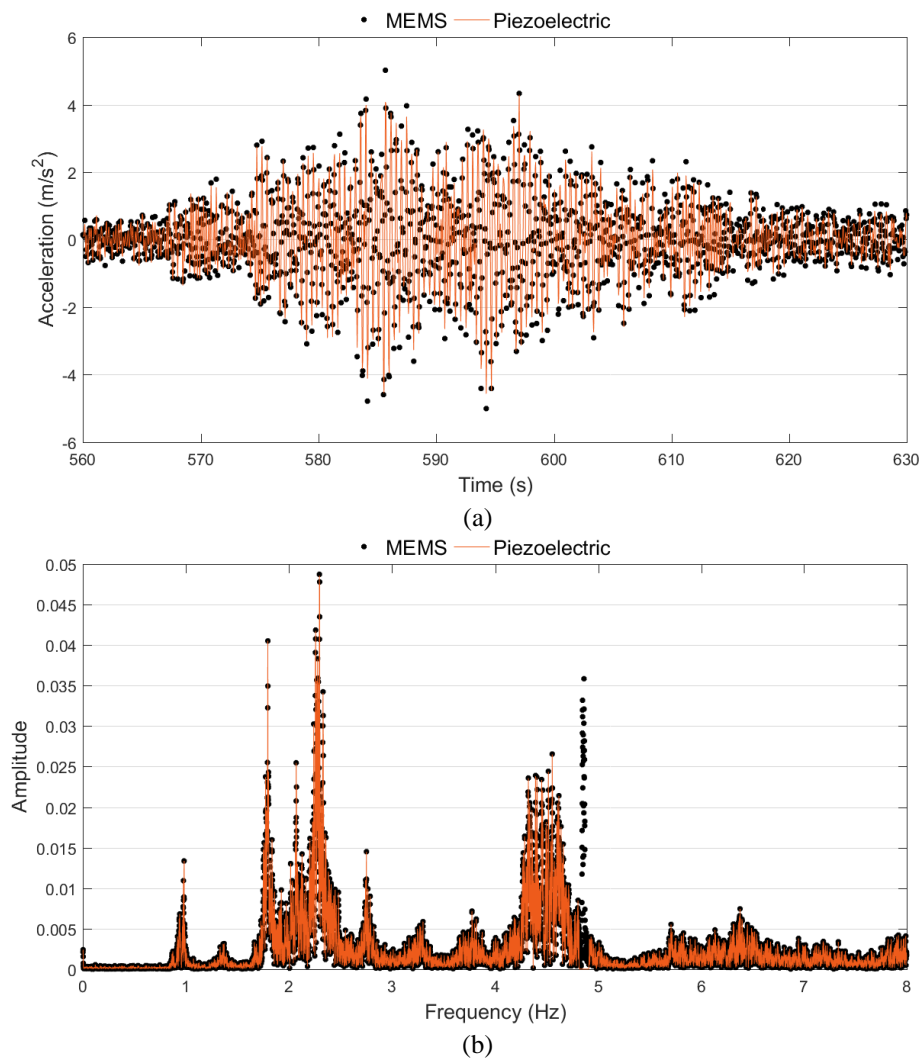


Fig. 8 Footbridge response registered with piezoelectric (blue) and A4 MEMS (red) accelerometers. (a) time domain and (b) frequency domain

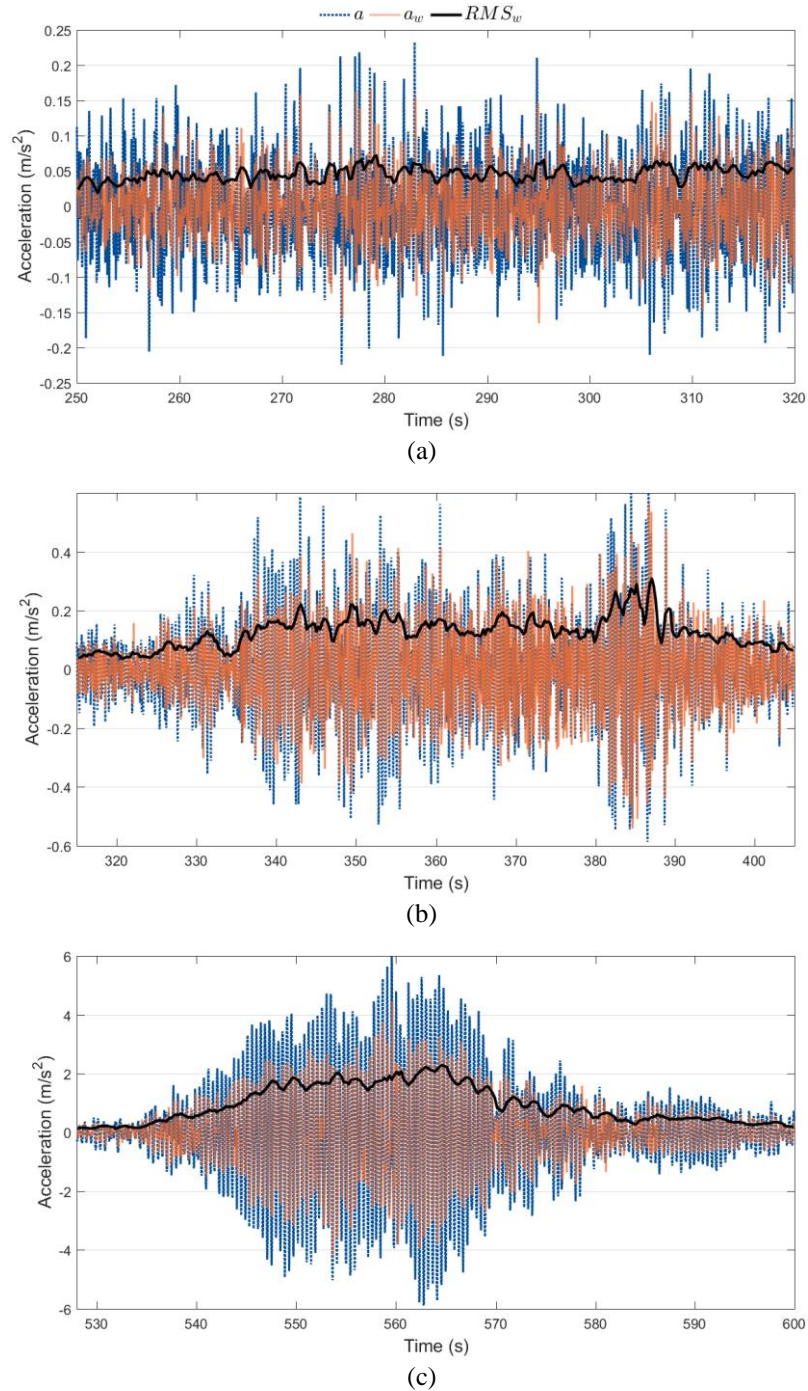


Fig. 9 A4 vertical accelerations and RMS trends when (a) no people crossing, (b) a group of 10 pedestrians crossing and (c) vandalism bouncing

4. Monitoring results

The operation of continuous monitoring systems leads to the accumulation of a huge amount of data that needs to be properly processed and analysed. For the accelerometer A4, vertical accelerations a_z , its weighted values a_{zw} (according to frequency weighting functions established in ISO 2631 for comfort criteria for standing pedestrian) and the weighted Root Mean Square (RMS) trend (1 s window) for three scenarios are presented in Fig. 9 during 75 s

(averaged time that takes to cross the footbridge). Scenario (a) is for the structure under environmental conditions (no people crossing), (b) is for a group of 10 pedestrians and (c) is for vandalism bouncing. Mean weighted RMS values are 0.0265, 0.145 and 0.643 m/s^2 respectively.

Fig. 10 shows, for former scenario (b), the three components X, Y and Z for the acceleration. Mean RMS values are 0.0191, 0.0527 and 0.173 m/s^2 respectively.

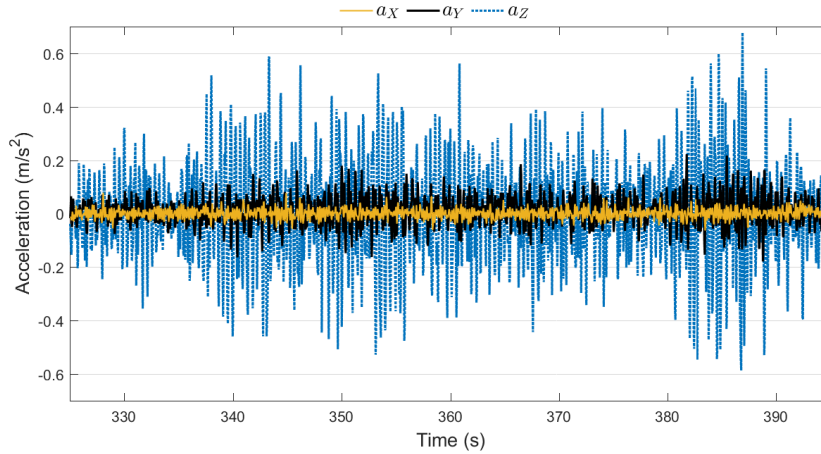


Fig. 10 A4 accelerations when a group of 10 pedestrians is crossing

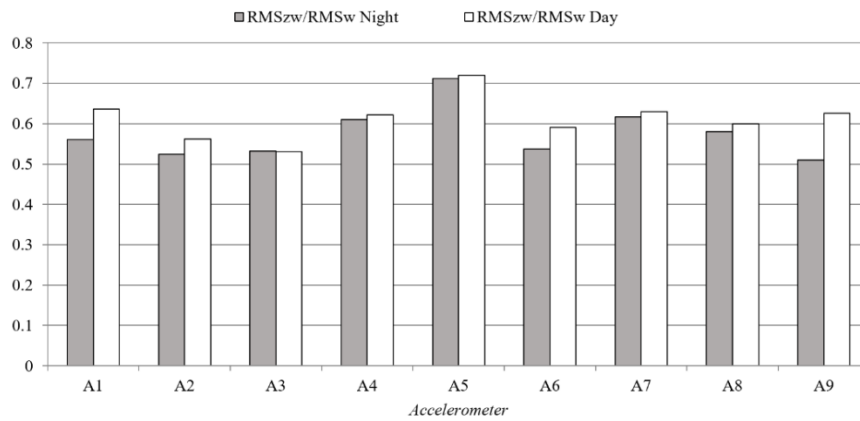


Fig. 11 Contribution of a_z to the acceleration magnitude

5. Post processed data

In order to investigate the effect of pedestrians on the response of this lively stress-ribbon footbridge under normal operational conditions, hourly data is processed to get a representative parameter for the whole hour. Fig. 11 shows the contribution (in magnitude) of the vertical direction (Z) to the whole acceleration vector (X, Y and Z). These values depend on the position of the accelerometers (from A1 to A9, in the upstream railing), but for all of them is around 60%, both during daylight and at night hours. This means that the vertical vibrations are the prevailing ones but horizontal vibrations are not negligible. During daylight, considered from 8 am to 5 pm, average use of the footbridge is more than one pedestrian at a time, being $RMS_{Zw} = 0.125 \text{ m/s}^2$. During the night (from 11 pm to 6 am) the RMS_{Zw} is only 0.063 m/s^2 .

Fig. 12 shows hourly parameters (peak, RMS_w for the 3 axis and RMS_{Zw}) for one selected day. Some patterns can be observed (mainly day/night use, with maximum values around 9 am and 6 pm and minimum around 1 am). Presented values have been obtained averaging the parameters for the upstream accelerometers (from A1 to A9).

Mean values through the year are 0.418 m/s^2 for peak acceleration, 0.0934 m/s^2 for RMS_w and 0.0532 m/s^2 for RMS_{Zw} .

Counting how many RMS_w hourly data are inside certain ranges, is easy to determine the percentages shown in Fig. 13. ISO 2631, annex C.2.3 establishes comfort reactions to vibration environments for public transport according to the following ranges in terms of RMS_w : Non-uncomfortable for less than 0.315 m/s^2 , a little uncomfortable between 0.315 and 0.63 m/s^2 , fairly uncomfortable between 0.5 and 1 m/s^2 , uncomfortable between 0.8 and 1.6 m/s^2 , very uncomfortable between 1.25 and 2.5 m/s^2 and extremely uncomfortable if greater than 2 m/s^2 . As no hourly RMS_w were registered over 1 m/s^2 , the three last ranges do not appear in the case under study. Additionally, the first range was subdivided in two at 0.15 m/s^2 , in order to get more detail information about comfortability. The resultant sub-ranges were classified as almost imperceptible up to 0.15 m/s^2 and noticeable between 0.15 and 0.315 m/s^2 . Note that the footbridge over the months has good serviceability conditions, with most of the time in the non-uncomfortable range. Also Fig. 13 shows averaged values for the monthly temperatures.

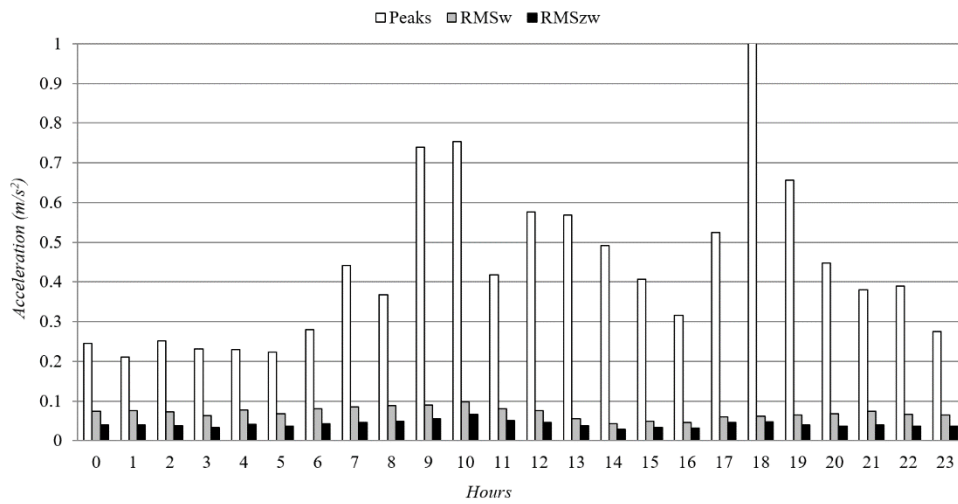


Fig. 12 Hourly parameters during a particular day

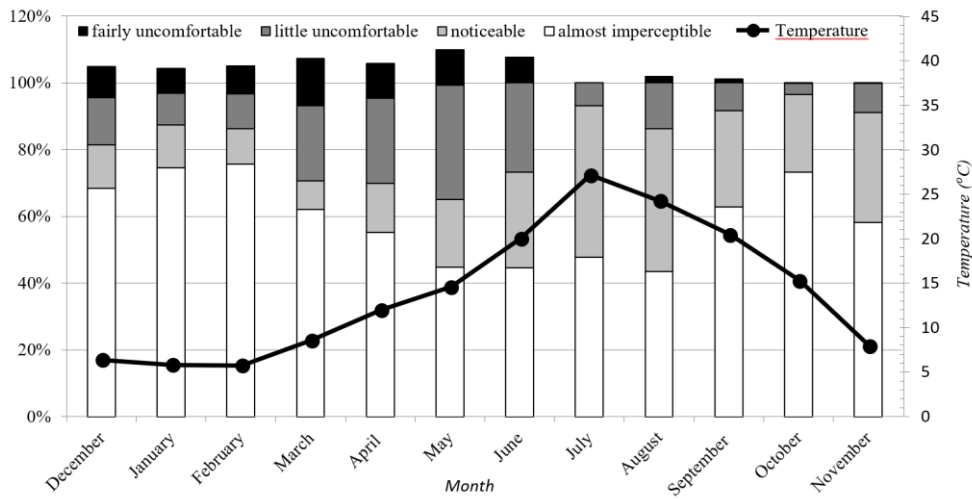


Fig. 13 Comfortability according ISO 2631

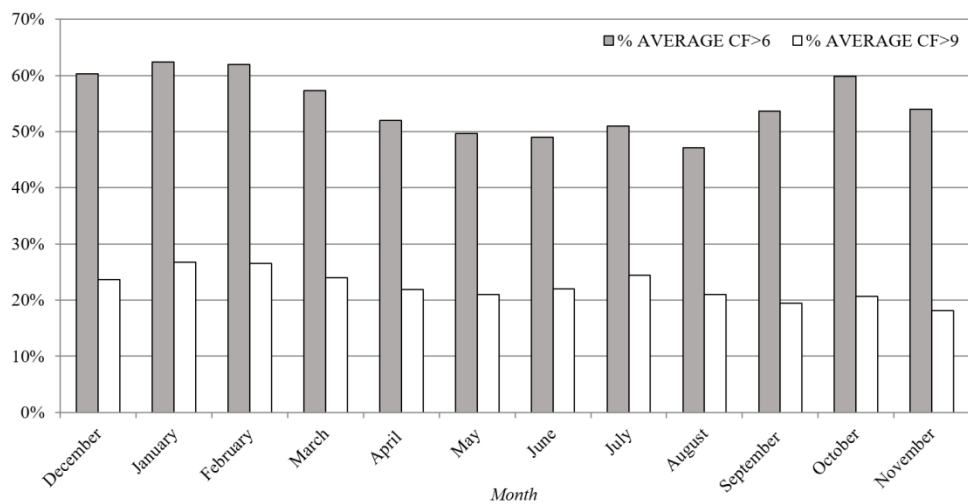


Fig. 14 Crest Factor exceeding 6 or 9

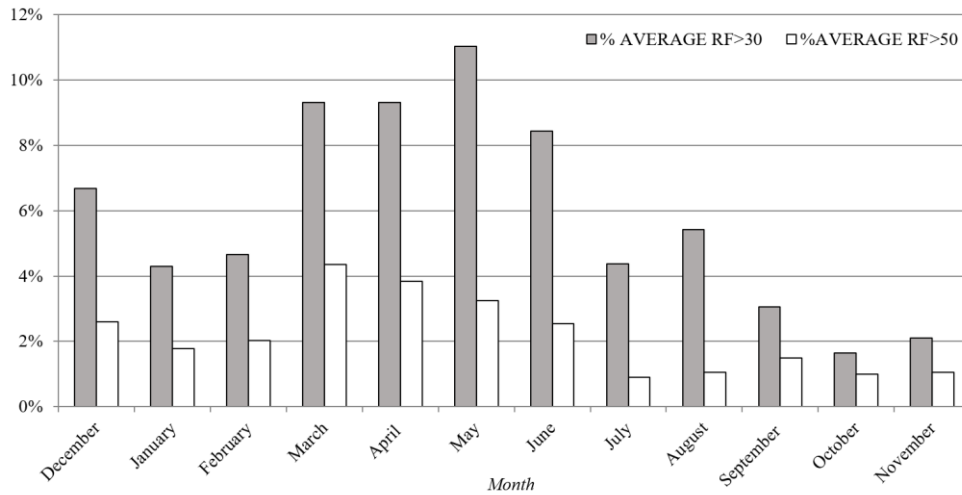


Fig. 15 Response Factor exceeding 30 or 50

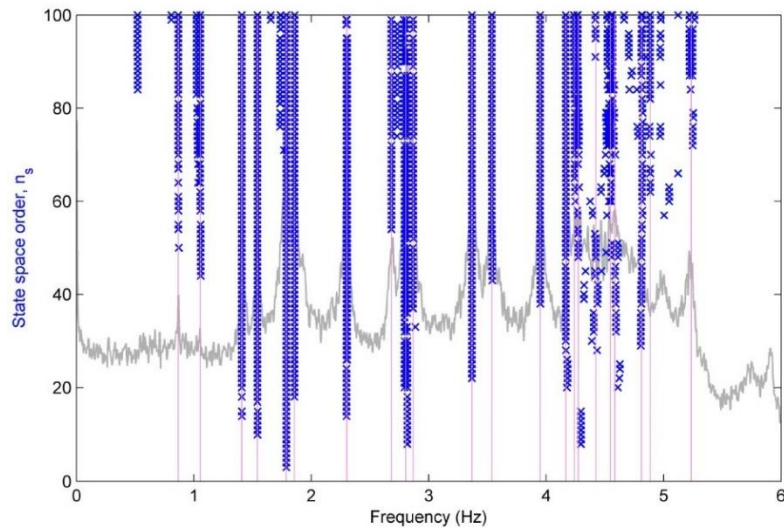


Fig. 16 Stabilization diagram using SSI algorithm up to order 100

ISO 2631 recommends the use of the RMS_w as serviceability parameter only if crest factors are below 6 (annex C.1.1.3) or 9 (part 6.2.2). Crest factor is the ratio between peak value and corresponding RMS_w during the same time of exposition (one hour has been taken). Fig. 14 shows that only around 20% of the time the crest factor exceeds the threshold of 9. For these cases, ISO 2631 recommends the use of additional parameters like the Maximum Transient Vibration Value (MTVV) or the Vibration Dose Value (VDV) to check serviceability criteria, although no ranges are depicted.

With the same objective of serviceability assessment, response factor is defined as the ratio between the RMS_w and the base curve defined in ISO 10137. The value of 0.005 m/s^2 is the reference (base curve) for vertical movements. Fig. 15 shows the percentages for R factor exceeding 30 and 50, computed in hourly RMS_w basis. The

values of 30 and 50 are usually considered as reference limits for comfortability. Again, the low percentages obtained reveal the footbridge is adequate to the pedestrian use regardless its slenderness and its easily noticeable movements.

6. Modal characterization

Besides the evaluation of the response presented in the previous sections, one of the main interest of the monitoring system is the modal characterization under different external factors (temperature, pedestrian use, etc.). For that, several operational modal analyses (output-only) were performed. Although more recent and powerful methodologies already exist (like the one presented in Sadhu *et al.* (2014)), a more traditional identification technique based on Stochastic Subspace Identification (SSI)

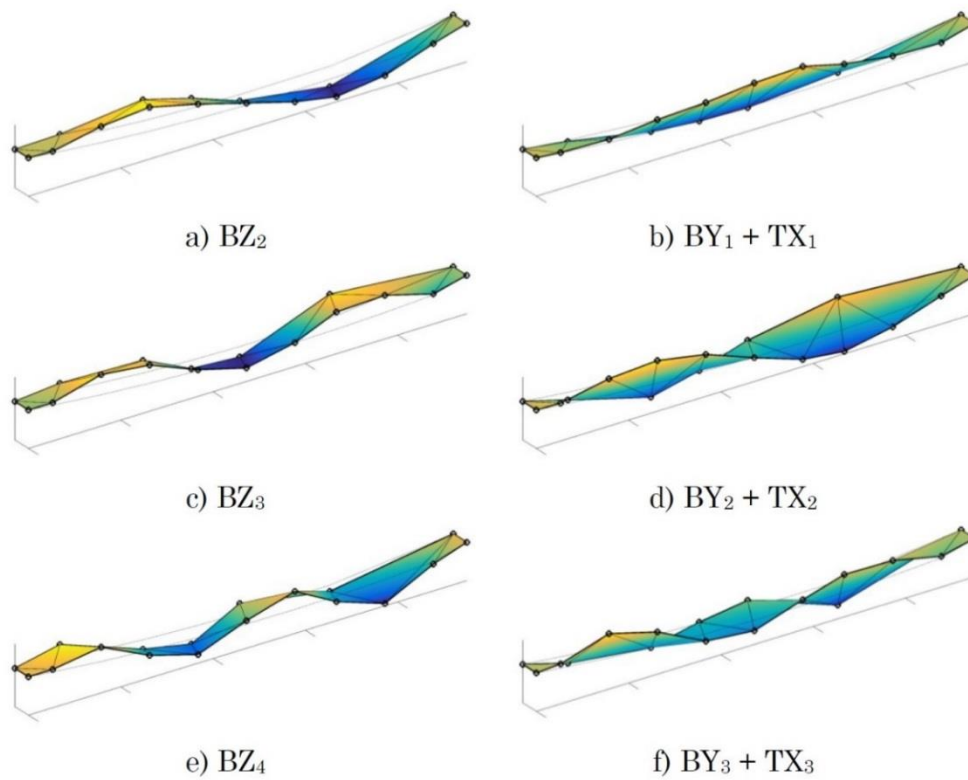


Fig. 17 First six mode shapes

Table 2 Experimental values of damping and frequency for the six first modes and their change with the temperature

Mode	ξ (%)	Frequency (Hz)			Mean	Frequency change (%)	
		5°C	20°C	35°C		% (5°C)	% (35°C)
BZ ₂	0.18	0.895	0.868	0.840	0.868	3.1	-3.2
BY ₁ + TX ₁	0.20	1.005	1.050	1.096	1.050	-4.3	4.4
BZ ₃	0.23	1.436	1.410	1.390	1.412	1.8	-11.4
BY ₂ + TX ₂	0.33	1.540	1.530	1.520	1.530	0.7	-0.7
BZ ₄	0.14	1.840	1.780	1.730	1.783	3.4	-2.8
BY ₃ + TX ₃	0.13	2.310	2.230	2.150	2.230	3.6	-3.6

(Ubertini *et al.* 2013) is enough for the intended purposes of this work. Fig. 16 shows modal identification diagram and Fig. 17 presents the first 6 modes obtained for very low occupancy and negligible wind loading.

For the modal mode shapes, the notation used is BZ_{*i*} for bending modes in the vertical XZ plane, BY_{*i*} for bending modes in the horizontal XY plane and TX_{*i*} for torsional modes around X axis. *i* is the number of antinodes of the corresponding mode. Generally, for these types of nonlinear structures, the frequency decreases when the temperature increases, but not a similar trend is evidenced for all the modes as seen in Table 2. Presented values were obtained from more than 1250 estimations based on hourly records.

7. Conclusions

The development and installation of a remotely control continuous vibration monitoring system on a stress-ribbon footbridge has been presented in this paper. This system is based on the use of low-cost triaxial MEMS acceleration sensors and was validated by comparing the response measured by the MEMS devices with conventional piezoelectric accelerometers mounted in a portable analyzer. As MEMS devices can measure gravity, spatial orientation is continuously adjusted by an automatic system based on Euler angles. These tests demonstrated that these low-cost sensors are a competitive alternative to traditional ones. Also, the system could be used to find correlations between the mechanical response and environmental data (Soria *et al.*

2017) and, in the long term, evaluate changes in the modal properties due to fatigue or abutment resettlements.

For accelerations over 0.02 m/s^2 there are not significant differences between both piezoelectric and MEMS sensors. For serviceability purposes and taking into account the lively structure under study (acceleration values over 0.05 m/s^2 when it is crossed by a single pedestrian, as shown in Fig. 9(a)), the monitoring proposal is not only more affordable but also a practical alternative.

Interesting operation results have been presented, including serviceability analysis and modal identification for the first six modes. The next objective is to implement an automated operational modal analysis in order to analyze the changes on the modal properties along the time. The influence of environmental factors (including temperature and wind) and pedestrian traffic density will be analyzed in order to remove these effects from the modal properties, as other authors (Moser and Moaveni 2013) propose. Thus, such modal properties may be used for structural damage detection which is the final goal to be achieved.

Acknowledgments

The authors wish to acknowledge the collaboration of the Valladolid City Council and the partial support through the Research Projects BIA2011-28493, DPI2013-47441, BIA2014-59321 (*Ministerio de Economía y Competitividad*, Spanish Government) and FPU16/01339 grant (*Ministerio de Educación, Cultura y Deporte*, Spanish Government).

References

- Brownjohn, J., Carden, E., Goddard, C. and Oudin, G. (2010), "Real-time performance monitoring of tuned mass damper system for a 183 m reinforced concrete chimney", *J. Wind Eng. Ind. Aerod.*, **98**(3), 169-179.
- Caetano, E., Silva, S. and Bateira, J. (2011), "A vision system for vibration monitoring of civil engineering structures", *Exp. Techniques*, **35**(4), 74-82.
- Casciati, S., Tenta, A., Marcellini, A. and Daminelli, R. (2014), "Long run ambient noise recording for a masonry medieval tower", *Smart Struct. Syst.*, **14**(3), 367-376.
- Ceylan, H., Gopalakrishnan, K., Kim, S., Taylor, P.C., Prokudin, M. and Buss, A.F. (2013), "Highway infrastructure health monitoring using micro-electromechanical sensors and systems (MEMS)", *J. Civil Eng. Management*, **19**(1), 188-201.
- Chen, Z. (2014), "Energy efficiency strategy for a general real-time wireless sensor platform", *Smart Struct. Syst.*, **14**(4), 617-641.
- Chen, Z. and Casciati, F. (2014), "A low-noise, real-time, wireless data acquisition system for structural monitoring applications", *Struct. Control Health Monit.*, **21**(7), 1118-1136.
- Gomez, H.C., Fanning, P.J., Feng, M.Q. and Lee, S. (2011), "Testing and long-term monitoring of a curved concrete box girder bridge", *Eng. Struct.*, **33**(10), 2861-2869.
- Guan, M. and Liao, W.H. (2006), "On the energy storage devices in piezoelectric energy harvesting", *Proceedings of the SPIE 6169, Smart Structures and Materials 2006: Damping and Isolation*, San Diego, California, United States, March.
- Lepidi, M. and Gattulli, V. (2012), "Static and dynamic response of elastic suspended cables with thermal effects", *Int. J. Solids Struct.*, **49**(9), 1103-1116.
- Moser, P. and Moaveni, B. (2013), "Design and development of a continuous monitoring system for the Dowling Hall Footbridge", *Exp. Techniques*, **37**(1), 15-26.
- Narros, A.J. (2011), "Pasarela peatonal Pedro Gómez Bosque sobre el río Pisuegra en la ciudad de Valladolid. Un nuevo récord de longitud en pasarelas colgadas de banda tesa", *Revista Técnica Cemento Hormigón*, **947**, 80-86.
- Orcesi, A.D., Frangopol, D.M. and Kim, S. (2010), "Optimization of bridge maintenance strategies based on multiple limit states and monitoring", *Eng. Struct.*, **32**(3), 627-640.
- Panigrahi, R., Bhalla, S. and Gupta, A. (2010), "A low-cost variant of electro-mechanical impedance (EMI) technique for structural health monitoring", *Exp. Techniques*, **34**(2), 25-29.
- Sadhu, A., Hazraa, B. and Narasimhan, S. (2014), "Ambient modal identification of structures equipped with tuned mass dampers using parallel factor blind source separation", *Smart Struct. Syst.*, **13**(2), 257-280.
- Shinozuka, M., Feng, M.Q., Chou, P., Chen, Y. and Park, C. (2004), "MEMS-based wireless real-time health monitoring of bridges", *3rd International Conference on Earthquake Engineering*, Nanjing, China, October.
- Soria, J.M., Diaz, I.M. and Garcia-Palacios, J.H. (2017), "Vibration control of a time-varying model-parameter footbridge: study of semi-active implementable strategies", *Smart Struct. Syst.*, **20**(5), 525-537.
- Strasky, J. (2005), *Stress Ribbon and Cable-Supported Pedestrian Bridges*, (1st edition), Thomas Telford Publishing Ltd, London, United Kingdom.
- Swartz, R.A., Lynch, J.P., Zerbst, S., Sweetman, B. and Rolfes, R. (2010), "Structural monitoring of wind turbines using wireless sensor networks", *Smart Struct. Syst.*, **6**(3), 183-196.
- Tan, T.D., Anh, N.T. and Anh, G.Q. (2011), "Low-cost Structural Health Monitoring scheme using MEMS-based accelerometers", *Proceedings of the 2nd International Conference on Intelligent Systems, Modelling and Simulation*, Phnom Penh, Cambodia, January.
- Tokogonon, C.A., Gao, B., Tian, G.Y. and Yan, Y. (2001), "Structural Health Monitoring framework based on Internet of Things: A survey", *IEEE Internet Things J.*, **4**(3), 619-635.
- Ubertini, F., Gentile, C. and Materazzi, A.L. (2013), "Automated modal identification in operational conditions and its application to bridges", *Eng. Struct.*, **46**, 264-278.

FC

Notation

The following symbols are used in this paper:

$\bar{a}_x, \bar{a}_y, \bar{a}_z$	=	average acceleration in each local axis x, y, z (m/s ²);
a_x, a_y, a_z	=	acceleration in each local axis x, y, z (m/s ²);
a_X, a_Y, a_Z	=	acceleration in each global axis x, y, z (m/s ²);
g	=	gravity acceleration (m/s ²);
$[R]$	=	coordinate transform matrix;
RMS_w	=	weighted Root Mean Squares;
RMS_{Zw}	=	weighted Root Mean Squares in the global axis Z;
α	=	accelerometer local pitch angle (°); and
β	=	accelerometer local roll angle (°).